AIAA Aviation
16-20 June 2014, Atlanta, GA
19th AIAA International Space Planes and Hypersonic Systems and Technologies Conference

Sensitivity of the Performance of a 3-Dimensional Hypersonic Inlet to Shape Deformations

Heather Kline*, Francisco Palacios† and Juan J. Alonso‡
Stanford University, Stanford, CA 94305, U.S.A.

Supersonic combustion ramjets, or scramjets, have the potential to facilitate more efficient transatmospheric flight and airplane-like operations of vehicles for space access. A scramjet is an airbreathing engine which uses the compression of air over the forebody and inlet to achieve the conditions necessary for supersonic combustion, using no mechanical compressor. Understanding the effects of shape deformations due to vehicle compliance is important for the robust performance of scramjets at on-design conditions where deformations may be large and have a significant effect, for multi-point operation where the shape of the vehicle changes with the varying pressure and temperature distributions, and for ensuring a lack of sensitivity to manufacturing tolerances. This paper will focus on the effects of shape deformations on the performance of the vehicle inlet under design conditions using high-fidelity simulations as well as response surface methodology.

Nomenclature

Variable Definition

A	Area
a	Speed of sound
f	Fuel mass flow rate ratio
g	Gravity
h	Enthalpy
I_{sp}	Specific Impulse
M	Mach number
P	Pressure
P_{tr}	Stagnation pressure ratio, a.k.a stagnation pressure recovery
q	Dynamic pressure
T	Temperature
γ	Ratio of specific heats
η_{AKE}	Adiabatic kinetic energy efficiency
θ	Shape parameter for combustor temperature profile

Subscripts

0	Freestream
2	Entrance to isoloator, end of inlet
3	End of isolator, entrance to combustor
4	Exit of combustor
10	End of nozzle/ expansion ramp
b	Burner
t	Total, or stagnation state

*Ph.D. Candidate, Department of Aeronautics & Astronautics, AIAA Student Member.
†Engineering Research Associate, Department of Aeronautics & Astronautics, AIAA Senior Member.
‡Associate Professor, Department of Aeronautics & Astronautics, AIAA Associate Fellow

Units

kPa	10^3 Pascals
m	meters
psf	pounds per square foot
s	seconds

I. Introduction and Motivation

SUPERSONIC combustion ramjets, or scramjets, have the potential to facilitate more efficient transatmospheric flight and airplane-like operations of vehicles for space access. A scramjet is an airbreathing engine which uses the compression of air over the forebody and inlet to achieve the conditions necessary for combustion, using no mechanical compressor. The combustion takes place at supersonic speeds. These engines operate in hypersonic conditions, ranging from Mach 5 to Mach 10 at current levels of technology. Ramjets have flown up through Mach 5.5, and at Mach numbers of around that magnitude it becomes more efficient to use supersonic combustion.[1] Recent flight tests of the HIFiRE, X-51 and X-43A have had success in achieving positive thrust, while also highlighting the difficulties of designing hypersonic airbreathing engines[1–3]. In addition to flight tests, many ground tests and simulations have been run using a variety of test facilities and computational tools. The challenges of hypersonic airbreathing propulsion include accounting for a high degree of shape uncertainty under the extreme thermal and aerodynamic loads experienced, preventing unstart of the engine, achieving a sufficient level of fuel mixing, integration with the vehicle, low-speed operation and transition through dual mode propulsion, and ensuring off-design operation. This paper will focus on the first of these challenges, on the effects of shape deformations on the performance of the vehicle inlet, and in particular on the deformations under pressure and temperature loads. This work is intended to lead to uncertainty quantification of vehicle performance.

Active cooling is often used to counteract the thermal loads experienced by hypersonic vehicles, particularly for metallic structures. When fuel is used as the coolant, the heating of the fuel can also increase burner efficiency. Reducing the amount of cooling needed may reduce costs, either through reducing the mass flow rate of coolant and/or through reducing the weight of the coolant system. For example, if cooling channels are used, they are machined into the skin of the vehicle, causing stress concentrations and requiring a larger structural weight as a result. In flight and ground tests of scramjet engines the fuel and cooling systems have been decoupled, for example in the X-43 Mach 10 flight test,[2] however in an ideal situation they would be linked and a vehicle designer would want to be able to estimate the potential trade off of allowing the wall temperature to vary.

Previous aerothermoelastic studies are detailed in References 4, 5, and 6. Aerothermoelasticity couples together the disciplines of aerodynamics, structural elasticity, and thermodynamics. A fully coupled system is computationally expensive, and low-fidelity approximations are often used for the aerodynamic model. In this work we have modeled the flow in high fidelity and simulated the structural deformation through an un-coupled structural model. The aerodynamic simulation results are used to determine reasonable pressure and temperature loads to apply to the structural model.

Additional work presented in this paper is the development of a response surface in Mach number, dynamic pressure, and three shape parameters has been developed using Reynolds-Averaged-Navier-Stokes (RANS) simulation output and the same geometry. The purpose of developing this response surface was to observe the performance variation under other, non-structural deformations. It was used in comparison to predicting the change in performance to computed structural deformations.

II. Description of the Physical Problem

A. Hypersonic Flow and Supersonic Combustion Ramjets

Hypersonic flow begins in the neighborhood of Mach 5, and is defined not with a specified Mach number but as the flight regime where a number of physical phenomena become more significant. These phenomena include thin shock layers where the shock lies very close to the surface of the vehicle, thick boundary layers which interact with the shocks and a large entropy gradient, and the possibility of chemically reacting flow and real gas effects.[7] In the region of Mach 5 the cost of decelerating air to subsonic speeds begins to outweigh

the cost of supersonic combustion. Combustion at supersonic speeds is more difficult to implement, and issues with residence time, sufficient mixing, and unstart become more significant. The inlets of scramjets need to compress the air sufficiently, while maintaining low drag and high efficiency. Highly uniform flow is often held to be desirable, however for greater fuel penetration there may be some advantages to a degree of cross flow. Under extreme pressure and heat, there is a higher degree of shape uncertainty. Hypersonic vehicles for access to space are required to operate under a very large range of flight conditions, accelerating to an altitude where rocket propulsion takes over. A diagram of a scramjet is shown in Fig. 1. This figure also identifies the stations 0-10 which will be used as subscripts to describe the state of the flow at those locations. Several numbers are left out of this figure for consistency with describing other engines, where there would be more components between the exit of the combustion chamber or burner and the nozzle.

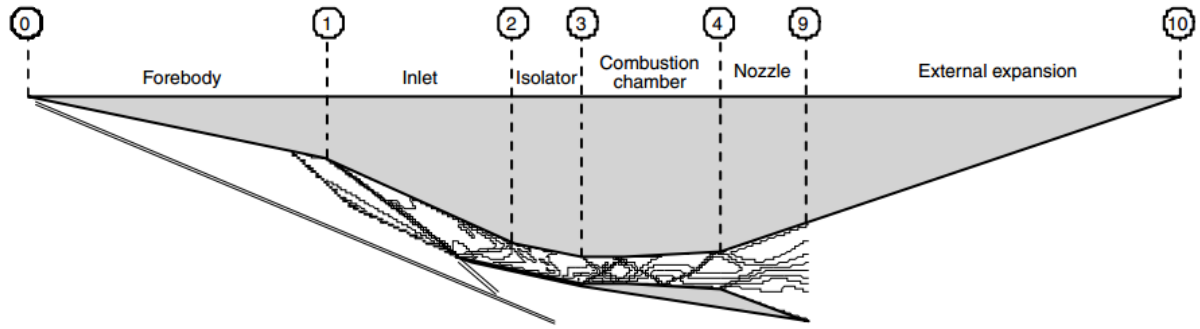

Figure 1: Scramjet flow path. Reproduced from Fig.1 of Ref. 8

B. Sensitivity of Hypersonic Inlet Performance to Shape Deformations

Accounting for the shape deformations of hypersonic vehicles due to vehicle compliance is important to their design for on-design or single-point performance where the deformations may be large and have a significant effect on the performance. This is also important to robust or multi-point operation where the shape of the vehicle changes with the varying pressure and temperature distributions. Under hypersonic conditions high temperatures are expected due to temperature increases over shocks and due to friction. Large magnitudes of pressure and shear force are also expected. Vehicle compliance is unlikely to be negligible due to the slender shape of a scramjet powered vehicle and due to the need to decrease the weight of the vehicle for improved efficiency. Aleatory uncertainty in the freestream flow conditions and therefore in the pressure, shear, and thermal load distribution contributes to uncertainty of the shape deformations. Manufacturing tolerances also add uncertainty to the shape of the vehicle.

The deformations of a vehicle geometry, in this case the inlet of a scramjet engine, can be simulated using Finite Element Methods (FEM). In a full aero-thermo-elastic simulation the CFD solution would be coupled with the solution of deformations due to the combination of thermal expansion and deflections due to pressure and shear forces. Previous aerothermoelastic studies are detailed in References 4, 5, and 6. Aerothermoelasticity couples together the disciplines of aerodynamics, structural elasticity, and thermodynamics. A fully coupled system is computationally expensive, and low-fidelity approximations are often used for the aerodynamic model. In this work we will not attempt a coupled model, but rather model the flow in high fidelity and approximate the structural deformation through an un-coupled structural model. The aerodynamic simulation results are used to determine reasonable pressure and temperature loads to apply to the structural model. While uncoupling the structural and aerodynamic models introduces an inherent inaccuracy relative to a fully coupled system, an attempt has been made to use realistic structural properties. In addition, the pressure distribution calculated on the deformed surface will be used to evaluate whether additional iterations in the structural deformations would be desired.

C. Description of the Geometry

The geometry investigated is a Rectangular-to-Elliptical-Shape-Transition (REST) scramjet inlet which was designed in the Hypersonic Airbreathing Propulsion Branch at NASA Langley. The associated study is

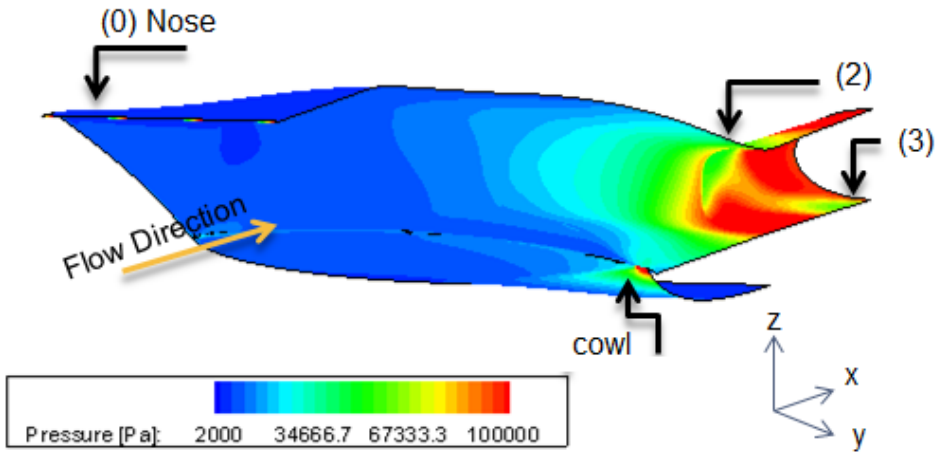

Figure 2: Modeled geometry: REST inlet cut along symmetry plane.

detailed in Ref. 9 and Ref. 10. The geometry investigated in this work is "case 17" from Ref. 9 , and the flow solutions used in the development of the response surface were generated using the same Computational Fluid Dynamics (CFD) model, VULCAN.[11] Selected flow cases were repeated in a second CFD suite, SU^2, which was the CFD suite used for the simulation of structurally deformed geometry. The method used to generate this inlet is described in more detail in Ref. 12 and Ref. 9. In summary, an axisymmetric compression field is generated that has the desired compression for the inlet, followed by using stream-tracing to form superelliptical cross-sectional inlets, which are then blended together with lofting. An approximate correction was then added with an assumption of negligible cross-flow. The compression field in this case used an expanding flow field with the desired properties, reversed the direction of flow and truncated the inlet. The design conditions for this inlet were freestream conditions of M_0=7, q_0=82.833 kPa (1730 psf) with a desired compression ratio of 37.55. The geometry is shown in Fig. 2. This figure shows one-half of the inlet and isolator, cut along the symmetry plane.

This inlet is 1.22 m long, with a cross-sectional area of 2.5795×10^{-3} m^2 at the end of the inlet and isolator geometry (station 3 in Fig. 1). One-half of the inlet/isolator geometry is simulated, and it is cut along the symmetry plane. The combustor geometry used was chosen for predicting favorable performance at a range of conditions using the model described in section C. The geometry consists of a channel with linearly increasing cross-sectional area. During development of the response surface an area ratio of 3 between station 4 and station 3, an overall length of 0.5 m and a constant-area section 0.1 m long was used. Higher values of thrust can be obtained, however other geometries were found to produce thermally-choked conditions in the combustor for some conditions. As the inlet geometry, and not the combustor, is the focus of this paper, a constant combustor geometry has been used for consistency, and to reflect the intention of evaluating the effects of unintended inlet geometry changes.

III. Implementation

This section will describe the methods used in this work. First the simulation methods for aerodynamics, structural deformation, and low-fidelity combustion and expansion will be described. This is followed by the methods used to implement deformation of the computational mesh for the flow simulation. The main quantity of interest for this work is the stream thrust of the scramjet calculated between stations 0 and 10 in Fig. 1, and the details of that calculation as well as other quantities tracked during this work will be described. The shape parameters and initial response surface generation will also be described. As an overall summary of the methods, the inlet and isolator, station 0 to 3, was simulated using Reynolds-Averaged-Navier-Stokes (RANS) model in two Computational Fluid Dynamics (CFD) frameworks. Deflections of the body were computed using NASTRAN^{TM}, and applied to the computational mesh use SU^2 tools.

A. Computational Fluid Dynamics

Two CFD programs have been used: the Viscous Upwind aLgorithm for Complex flow ANalysis (VULCAN) version 6.1,[11] and Stanford University Unstructured (SU^2).The turbulence model was in VULCAN was Wilcox $k-\omega$, while in SU^2 the SST $k-\omega$ turbulence model was used. For both cases a turbulence intensity of 0.001 and a turbulent to laminar viscosity ration of 0.01 was used. While using VULCAN a multi-block structured mesh provided by Paul Ferlemann with approximately 2.7 million cells was used. For transitioning to the open-source software SU^2 a new mesh had to be developed to accommodate the single-block requirement. This unstructured mesh required a larger number of cells, on the order of 6 million.

SU^2 uses the Finite Volume Method (FVM) to solve partial differential equations including the Reynolds-Averaged-Navier-Stokes (RANS) equations and the Euler equations. This software suite uses unstructured meshes to discretize the volume. In the RANS equations a turbulence model is used to account for the Reynolds stresses. The one-equation Spalart-Allmaras and two-equation SST k-omega turbulence models are available. The SST model was used in this work as it is more similar to the turbulence model used in VULCAN, the Wilcox k-omega model. VULCAN is described in more detail in Ref. 11. SU^2 is an open-source software under development in the Aerospace Design Lab at Stanford University.[13]

B. Structural Deformations: Finite Element Analysis

Scramjet inlets encounter an extreme heating environment due to frictional forces. For this reason, they are often designed with actively cooled walls. Therefore the structural deflections are influenced by both the material expansion due to thermal loads and the force due to pressure loads. MSC NASTRAN^{TM}and associated tools were used to perform the structural deformation estimates. Thermal expansion and deflections from pressure distribution were calculated using the linear solver, SOL101 of NASTRAN^{TM}. The structure was of shell-and-beam construction with material of properties of Inconel-718.[14] In order to produce reasonably realistic deformations, the optimization utility of NASTRAN^{TM}was used to minimize the weight of the structure while constraining the maximum stress to be less than $\frac{1}{2}$ of the 0.2% yield strength. The optimization was conducted under the loading case of: a one-dimensional pressure distribution extracted from a flow solution at dynamic pressure of 82 kPa (1730 psf) at Mach 7 and wall temperature profile constructed by taking the temperature profile near the wall from the CFD solution and subtracting a constant value of 698 degrees in order to obtain an average wall temperature of 300 degrees Kelvin. This represents an assumption that the cooling system of the vehicle has been able to achieve the desired average temperature, but that the change in temperature between the nose of the inlet and the combustion chamber is similar to the uncooled state. This temperature distribution is illustrated in Fig 19.

The structural mesh is shown if Fig. 3. The optimization of the structure resulted in a shell thickness of .013139m and a bar dimensions with a flange width of 0.03m, a web thickness of 0.01211m and height of .10236m. While load conditions changed, these dimensions were used for all cases for consistency. As the goal of this paper is more in line with investigating the performance change under varying conditions rather than optimization, this initial solution for the structure is used with the note that in a realistic design cycle the structure would require further iterations.

C. Combustion and Expansion Models

Combustion was modeled using quasi-one-dimensional channel flow equations with heat addition, following analysis developed in Ref. 15 and Ref. 16. The associated ordinary differential equation is shown in Eqn. 1. Flux conserved one-dimensional values from the CFD were used as the initial conditions to solve this ODE numerically. A constantly-increasing area with an entrance to exit ratio of 1:10 was used as smaller ratios were found to produce thermally choked flow in some cases.

$$\frac{dM}{dx} = M\left(\frac{1+\frac{\gamma_b-1}{2}M^2}{1-M^2}\right)\left\{-\left(\frac{1}{A}\frac{dA}{dx}\right)+\frac{1+\gamma_b M^2}{2}\left(\frac{1}{T_t}\frac{dT_t}{dx}\right)\right\} \tag{1}$$

Heat addition was included using an assumed stagnation temperature profile defined in Eqn. 2. This profile is defined by an assumed shape parameter, θ and assumed burner efficiency, η_b. Following the values used in Ref. 15, $\eta_b = 0.8$ and θ=5.

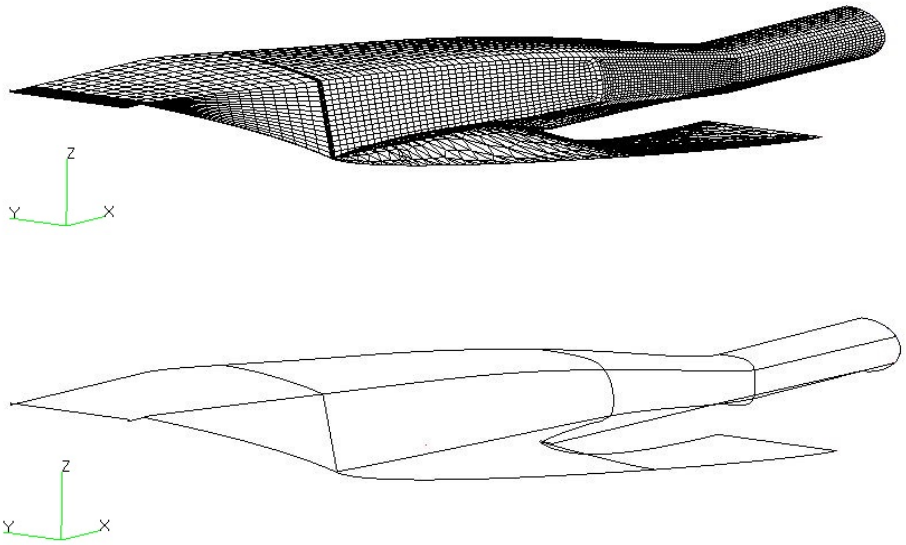

Figure 3: Structural mesh. The second image shows the location of bar elements.

$$\tau(x) = 1 + (\tau_b - 1)\left\{\frac{\theta\chi}{1+(\theta-1)\chi}\right\}$$
$$\tau_b = \frac{T_{t4}}{T_{t2}} \tag{2}$$
$$\chi = \frac{x - x_3}{x_4 - x_3}$$

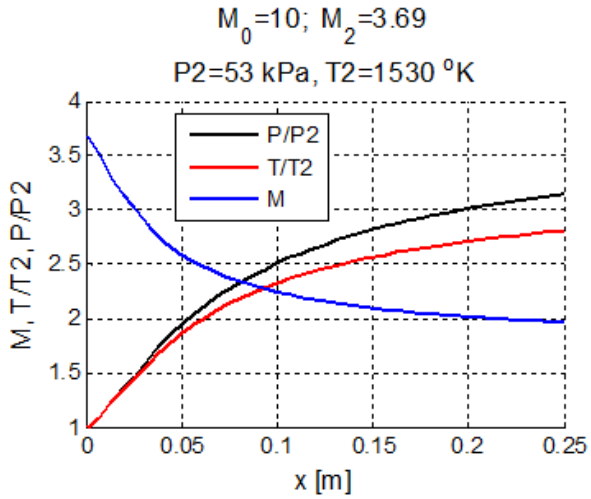

Figure 4: Example output from combustion model. Initial conditions were drawn from an inviscid model of a simple two-dimensional inlet in Mach 10 flow.

Adiabatic expansion to freestream pressure was assumed for the calculation of station 10 values based on the station 4 values computed from this combustion model.

In order to use these models, one-dimensional values had to be extracted from the high-fidelity flow solutions. Flux averaging was used to find the one-dimensional flow variables which produce the same flux

of momentum, mass, and energy as the flow at the 2-dimensional surface of the inlet exit (station 3 in Fig 1). Flux averaging equations can be found in Reference 17.

D. Mesh Deformation

Sculptor^{TM} software was used to implement mesh deformations for the initial response surface. Within this software, volumes surrounding a mesh are defined by the user to encompass only the portions of the mesh that are desired to change. Groups of control points within these volumes are defined as the design variables. Limitations to the magnitude of deformations were encountered due to the occurrence of negative-volume cells. This mesh deformation software was used for the initial response surface generation. Additional methods of mesh deformation exist within SU^2 and were used in the structural deformation cases. The structural deformations exported from NASTRAN^{TM}were interpolated onto the surface points of the CFD mesh. The deformation of the volume mesh was computed using a structural analogy with the stiffness of the cell edges proportional to the cell volume. It should be noted that some care needs to be taken in the creation of meshes which behave well both for CFD and for mesh deformation to avoid the creation of negative-volume cells and poor quality deformed meshes.

E. Quantities of Interest

Several quantities of interest were tracked during the course of this work. The most easily interpreted by the reader are likely to be the thrust and the specific impulse, and these have been focused on the most. Additional quantities of interest used as indications of the performance of the scramjet inlet are: the adiabatic kinetic energy efficiency, the inlet capture area, and the pressure ratios across the inlet. While only the inlet is simulated with high fidelity during this study, the motivation is to increase the performance of the overall propulsion system of a hypersonic vehicle. Therefore, estimates of the thrust and specific impulse, I_{sp} were calculated using averaged values of the flow properties at the end of the inlet. The equation for thrust is shown in Eqn. 3 and is based on the momentum flux of the air passing through the engine. The derivation of this equation can be found in Ref. 18. The definition of I_{sp} is shown in Eqn. 4. The quantities with subscript 0 are the freestream values, and the quantities with subscript 10 are values at the exit of the expansion ramp, as shown in Fig. 1. The former is specified, and the latter is computed as described in Section C. In these equations M is the Mach number, P is the static pressure, T is the temperature, f is the mass flow fraction of fuel:air, a indicates the speed of sound, $\dot{m}$ is the mass flow rate, and subscripts indicate the location along the flowpath as shown in Fig 1.

$$Thrust = \dot{m}_0 a_0 M_0 \left((1+f)\frac{M_{10}}{M_0}\sqrt{\frac{T_{10}}{T_0}} - 1 \right) + \frac{A_{10}}{A_0}\left(\frac{P_{10}}{P_0} - 1\right) \tag{3}$$

$$I_{sp} = \frac{Thrust}{\dot{m}_f g} \tag{4}$$

The adiabatic kinetic energy efficiency, η_{AKE}, is a measure of how much of the kinetic energy of the flow has been lost between the freestream flow and the end of the inlet, though comparing the freestream kinetic energy and the theoretical kinetic energy the flow at station 3 would have if it were expanded isentropically to freestream pressure. The definition of this quantity is shown in Eqn. 5. In this equation h_2' is the static enthalpy that the flow would have if it were expanded isentropically from the conditions at station 3 to the freestream pressure.

$$\eta_{AKE} = \frac{h_{t0} - h_2'}{h_{t0} - h_0} \tag{5}$$

The capture area, A_0 was used in the calculation of the thrust. In order to extract this information from the flow solution, a streamline was traced from the cowl tip back upstream to the entrance plane of the volume. The difference in height between the streamline and the nose of the inlet was used as the height of the capture area. An illustration of a sample streamline is shown in Fig.5. In thrust calculations for the results of structurally deformed geometry, the capture area was computed via conservation of mass between the freestream flow and the end of the isolator. The uniformity of the flow entering the combustor at station 3 is of interest as in a real engine can have a significant effect on the efficiency of mixing and combustion. While the calculation of thrust in this paper did not account for such effects, measures of nonuniformity were tracked during the development of the response surface. Due to corner flows it is possible for significant

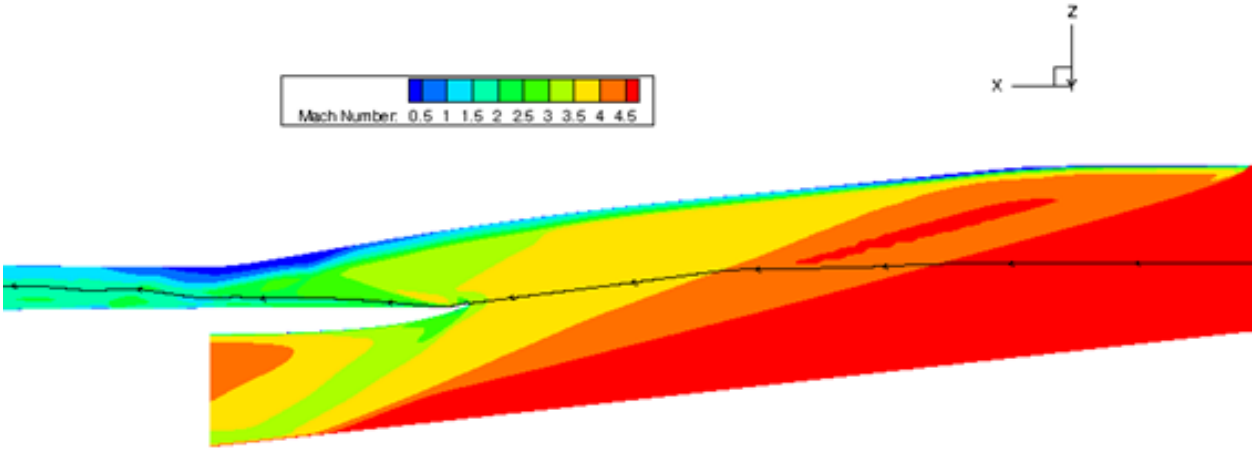

Figure 5: Illustration of capture area definition. The streamline shown in this figure is defined by the location of the cowl lip. Flow is from right to left.

counter-rotating vortices to form in the inlet, and at off-design conditions interactions of shocks and boundary layers cause additional nonuniformity. Measures of nonuniformity were output by the CFD program, and additional post-processing of the flow solutions.

F. Independent Variable Definition

The variables used for the response surface were the freestream Mach number M_0, the freestream dynamic pressure q_0, and three shape parameters which will be described shortly. Angle of attack was neglected in order to reduce the necessary number of flow solutions.

Nine shape deformation parameters were chosen initially, based on a combination of observations of the viscous flow solution of the baseline geometry and assumptions about parameters which would be likely to affect performance. Examples of the former are the "warps" and "central ridge" illustrated in Fig. 6. The central ridge parameter displaces a group of control points vertically along the centerline of the upper surface of the inlet for a large portion of the length, with the intention of counteracting the streamwise vortices which form in this inlet both on-design and for some off-design conditions. The warps cover the same region, providing deformations which are defined by a single control point for each of the five warps. The length of the inlet was varied with two parameters, one stretching the front of the inlet, and the other stretching the nearly constant-area portion which exhausts to the isolator. These are labeled "Entrance Length" and "Exit Length" in Fig. 6 respectively, and are controlled through translating planes of control points. Lastly, the plane at the point where the inlet begins to have a constant area, identified as "Convergence Location" (where the area converges to a constant value, or the entrance of the isolator), was translated horizontally as an additional control on the aspect ratio and relative lengths of the converging and constant-area sections of the inlet.

A screening of experiments was conducted to choose the most important parameters. This screening was conducted using MATLAB^{TM}[19] functions to define a fractional factorial design and conduct the analysis of variance after all simulations had been completed. With maximum ranges for deformations defined by trial and error to avoid cases with negative volume cells, a matrix of deformations was imported into Sculptor^{TM}[20] which exported a set of deformed meshes. These meshes were then used with VULCAN to find the flow solutions and output variables of interest. MATLAB^{TM}analysis of variance was then used to compare the statistical significance of the various input shape parameters. Main effects through two-way interactions were included in the ANOVA. A number of outputs were considered, including the stagnation pressure recovery, measures of flow uniformity, and thrust. All factors were found to have a statistically significant effect on at least one output.

The design parameters were reduced to only the entrance length, the central ridge, and a combination of the second and third warps from the front. Two of the warps were combined since they were found to

be of approximately equal significance and including both individually would have increased the number of parameters in the response surface.

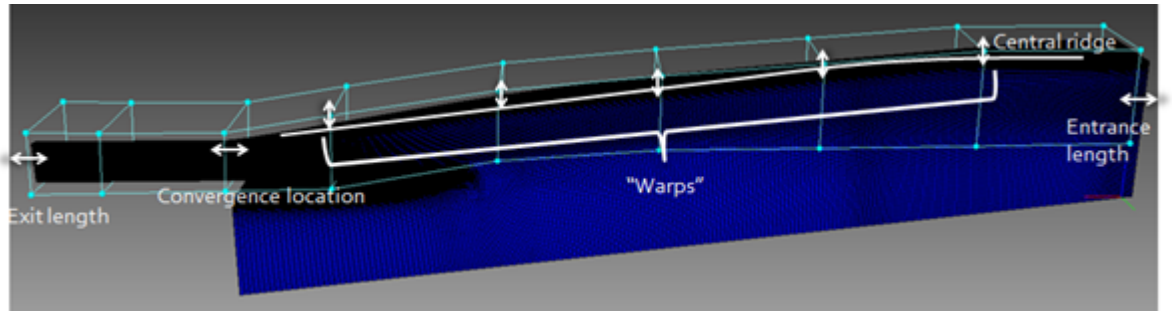

Figure 6: Illustration of the various deformation parameters used for the screening of experiments.

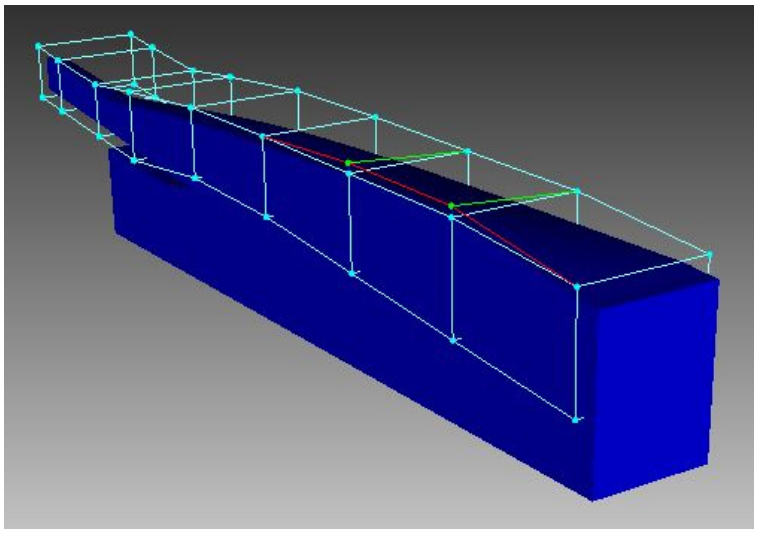

Figure 7: "Warp" parameter deformed 0.01 meters

G. Response Surface Generation

As nonlinearity is expected in this problem a second-order polynomial response surface was chosen for initial investigations. The response surface was designed using 40 training points arranged in a Latin Hypercube with five variables. The five variables were three shape parameters described in Section F, and the two remaining variables were the freestream dynamic pressure, q_0, and Mach number, M_0. The ranges for the shape parameters were +/- 0.02 meters, which was found to be the largest deformation which could be accomplished while reliably avoiding negative-valued grid cells and is representative of expected shape variations. M_0 ranged from 5 to 7, and q_0 ranged from 50 kPa to 100 kPa. These ranges were chosen to encompass a large but reasonable range around the design flight condition which was used for the baseline geometry. An additional 20 testing points in a Latin Hypercube design were used as test points. The residuals computed from these test points as well as the statistics on the original training points give an indication of response surface accuracy. The residuals are computed as the difference between the quantity predicted by the high-fidelity CFD and the quantity predicted by the response surface, $r = y - \hat{y}$.

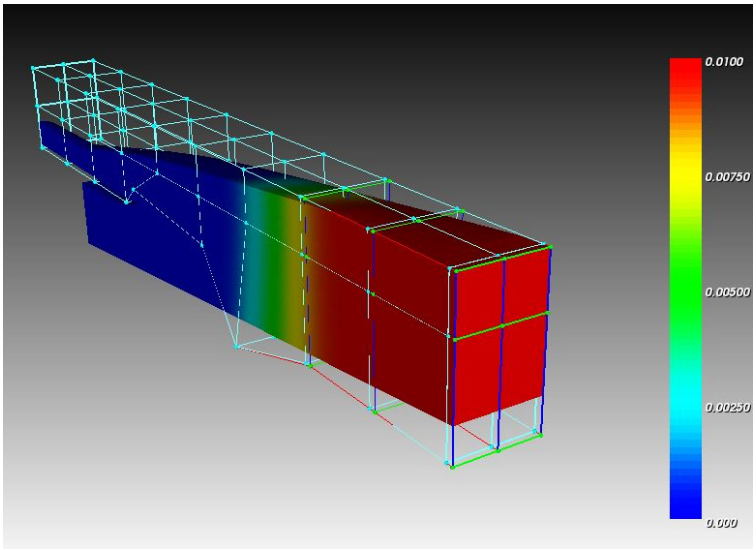

Figure 8: "Entrance Length" Parameter deformed 0.01 meters

IV. Results

A. CFD Verification

The initial analyses were conducted using VULCAN. Furthere analysis was conducted with SU^2. These tools, and their tradeoffs, have been discussed in preceding sections. In this section we examine how closely the results of these codes matched each other. The results presented compare simulations at a Mach number of 7 and a dynamic pressure of 75 kPa. Fig. 9 shows the static pressure along the inlet upper surface at the centerline, or symmetry plane, of the inlet. Fig. 10 and Fig. 11 show the static pressure and Mach number on a horizontal line extending from the freestream flow through the center of the inlet. The flat portion in each of these plots between x = 0 and $x \approx 0.5$ corresponds to freestream conditions. These results are quite close, especially considering that the simulations were conducted not only on different CFD codes, but also on different meshes. VULCAN uses structured, multiblock meshes while SU^2 utilizes unstructured meshes and requires a single-block mesh. Other differences between these CFD codes are detailed in Section III.A. The x-axis in these plots is the axial distance in meters from the nose (station 0) of the inlet. X=1.22 is station 3 of the inlet. We can see that the largest differences in the results occur in the isolator, or constant-area portion of the inlet where there are significant 3-dimensional effects.

B. Structural Deformations

In this section we summarize the structural deformations found under various conditions. Table 3 lists the deformation of the tip of the inlet, where the maximum deflection is experienced in every case. The numbers in this table were obtained from an initial structural model with the same mesh layout but different thicknesses; they are presented to show the difference between different types of load conditions - only the temperature profile case was applied to the final version of the structure. The deformation only pressure loads are applied are an order of magnitude smaller than cases with both pressure and temperature applied. The x-direction is positive in the flow direction, so a negative value indicates that the inlet has stretched to a longer length. The temperature load is drawn from a temperature distribution extracted from a flow solution and adjusted to have an average of 300^oK. 300^oK was the wall temperature assumed in the CFD simulation. Reference 21 includes results which indicate that cooling may produce a temperature profile of the same shape as the uncooled profile. Results of this reference included a comparison of cooled and uncooled wall temperature in a channel simulating a scramjet combustor cooled by hydrogen. Therefore, rather than taking a constant temperature as the applied thermal load for the structural model, a temperature profile of the same shape as found within the boundary layer of the flow solution is used. A large amount of variation in temperature is found, and the average temperature is much higher than the applied wall temperature.

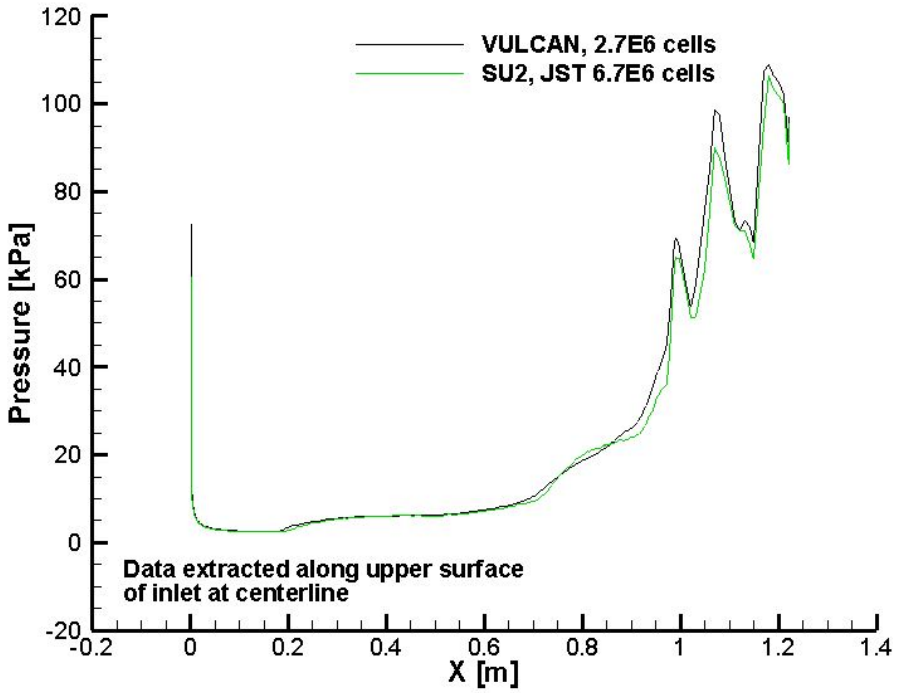

Figure 9: Pressure profile along centerline of the inlet

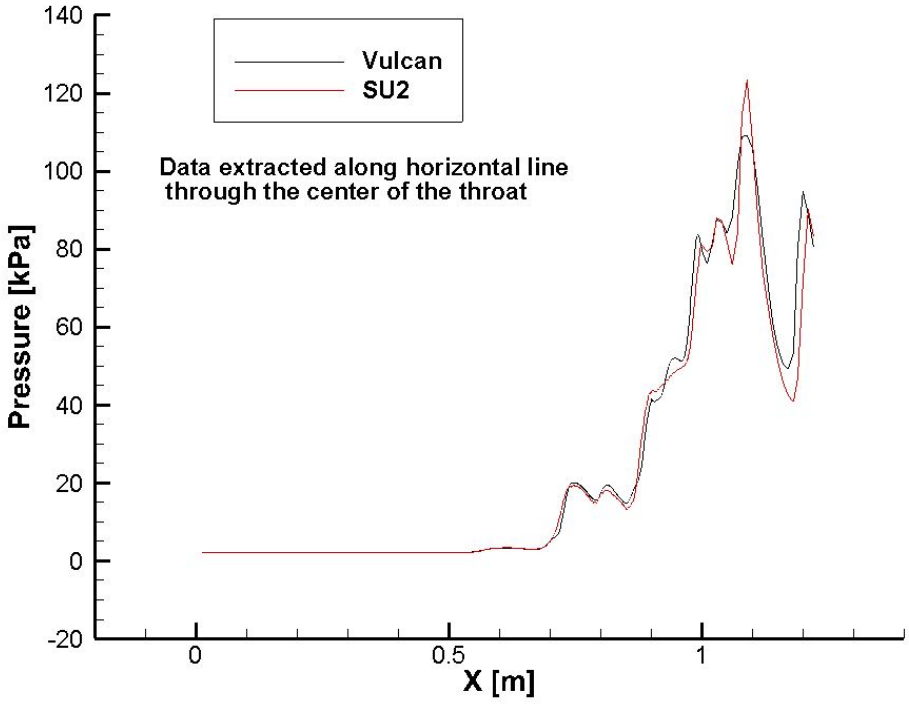

Figure 10: Pressure profile along a horizontal line through the center of the throat

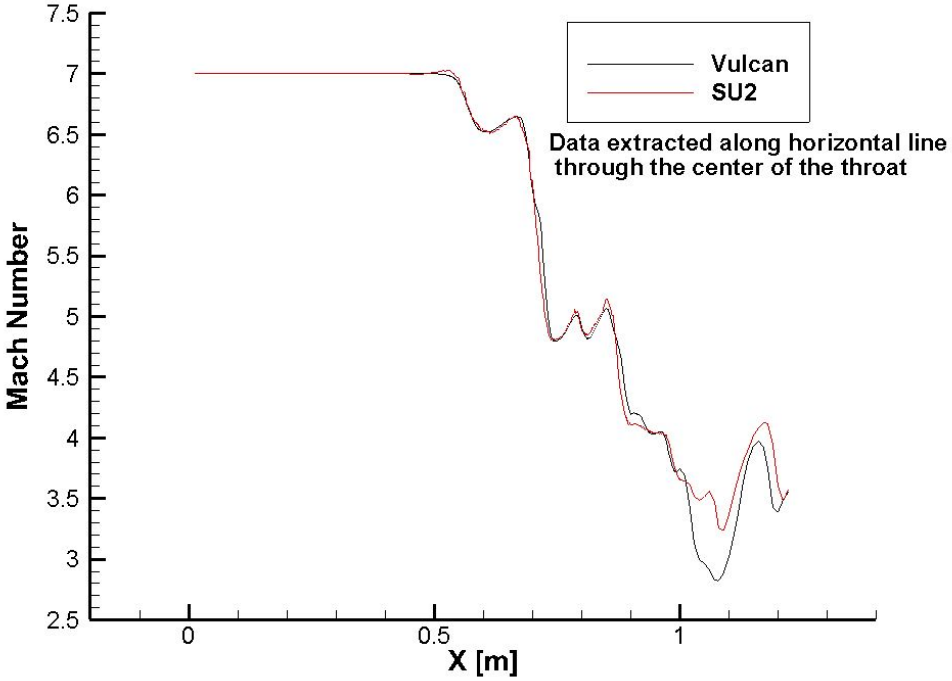

Figure 11: Mach profile along centerline of the inlet

Although not considered in this work, it may be relevant to consider varying wall temperature in CFD simulations in this regime due to the large temperature gradients encountered. As there is a significant deformation compared to the pressure-only result when the average temperature is the same as the initial temperature, this appears to be an effect which warrants consideration. Figures 12-13 illustrate that the deflections are nearly linear with the average temperature of the wall. A sample deflection is illustrated in Fig. 14. The deformation in this figure is not to scale. While the pressure forces would tend to deflect the nose upward, the more dominant thermal expansion causes the inlet to bend downward.

Table 1: Tip Deflection Results

Pressure	Temperature	Tip Deflection	
		x	z
Pressure, $q_\infty = 82kPa$	no change	2.14E-05	0.000165
Pressure, $q_\infty = 75kPa$	no change	1.939E-05	0.00015
Pressure, $q_\infty = 82kPa$	temperature profile - average of 300 degrees	-0.000984	-0.00778

C. Response Surface Generation Results

1. Results of Screening Experiment

A screening of experiments was conducted to choose the most important parameters in order to reduce the number of points required to generate a response surface. This screening was conducted using a fractional factorial design to choose the levels of each variable. With maximum ranges for deformations defined by trial and error to avoid cases with negative volume cells, a matrix of deformations was imported into Sculptor^{TM} which exported a set of deformed meshes. These meshes were then used with VULCAN to

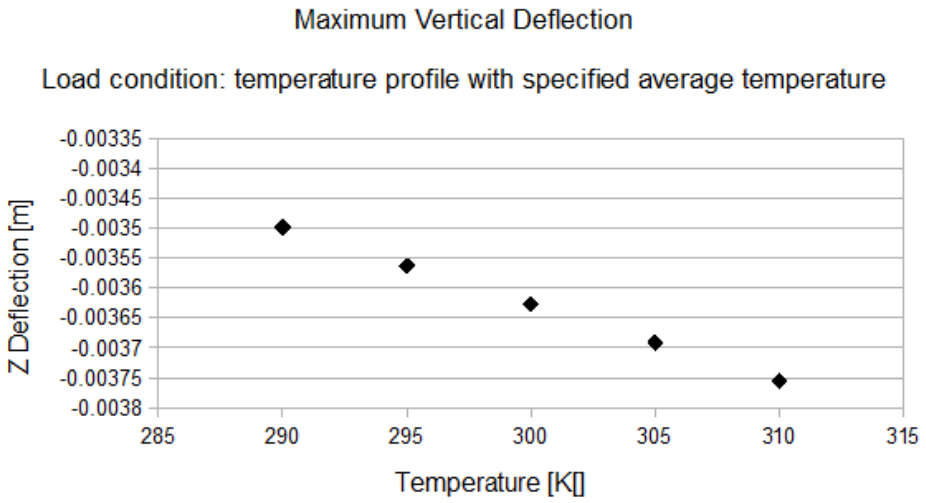

Figure 12: Maximum vertical deflection (deflection of the inlet nose) plotted against average temperature of the applied temperature profile.

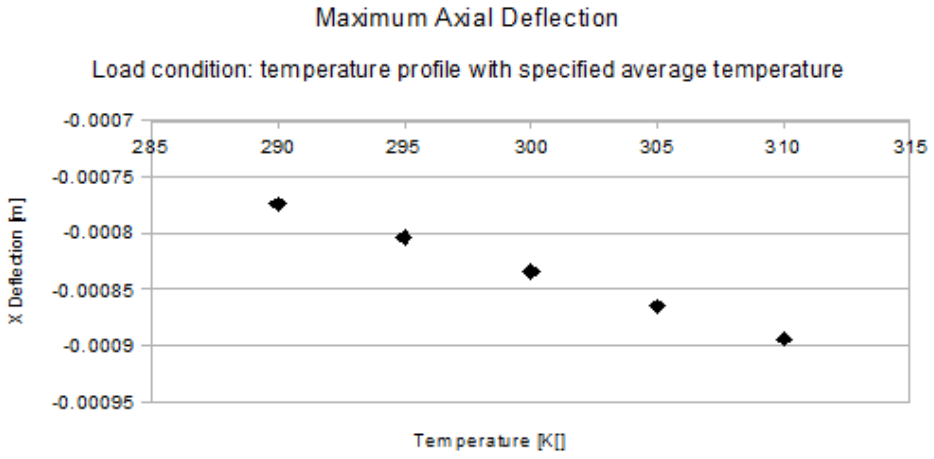

Figure 13: Maximum axial deflection (deflection of the inlet nose) plotted against average temperature of the applied temperature profile.

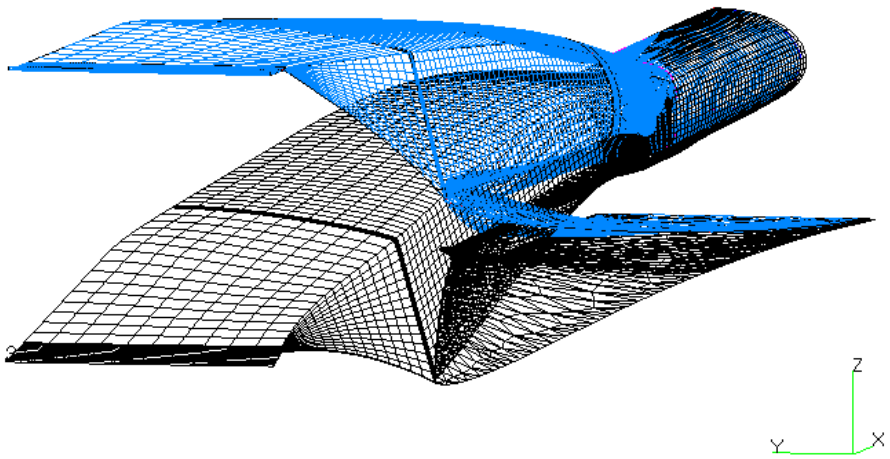

Figure 14: Deflection of the structure. Magnitude is significantly exaggerated: maximum deflection is 3.64E-3m, overall length is 1.22m.

find the flow solutions and output variables of interest. Analysis of variance was then used to compare the statistical significance of the various input shape parameters. For thrust, the most significant factors were two of the warping parameters nearest the front of the inlet, the entrance length, and the central ridge. These parameters are illustrated in Fig. 6.

2. Response Surface Equations

Figure 15a shows the contour plots of the thrust as estimated using quasi-one-dimensional analysis, described in Section III.E, and the flux-conserved average values of the conditions at station 3 as defined in Fig. 1, plotted against two of the shape parameters. Assuming that the simple model of thrust is sufficient, this plot implies that the highest thrust possible lies outside of the range of deformations studied in this response surface. This does not necessarily mean that an optimal point is outside of this range, for example if constraints are active or if the objective function includes other quantities. Comparison between Fig. 15a and Fig. 15b shows that maximum stagnation pressure ratio and maximum thrust do not coincide. The stagnation pressure contours, in Fig. 15b, reveal an apparent saddle point in the neighborhood of the initial geometry. We can also see that in both of these measures the conditions closest to the design conditions of the inlet achieve the largest thrust and largest stagnation pressure ratio at the intial geometry.

The adiabatic kinetic energy efficiency, which has been desribed in Section III.E., is plotted in Fig. 16a. Although both η_{AKE} and P_{tr} are measures of the efficiency of an inlet, the contour plots exhibit distinct behavior do not have coincident maxima.

Although the plots of thrust and I_{sp} in Fig. 15a and Fig. 16b exhibit different behavior, they agree on the maximum value lying to the right or upper right hand corner of the region modeled by the response surface. The static pressure ratio contours shown in Fig.17a, in contrast to the stagnation pressure ratio, also agrees with the thrust and I_{sp} in terms of the general direction of a maximum.

D. Response Surface Error Analysis

The use of regression allows analysis of the residuals from the points used to develop the response surface. The points used for the response surface and residuals are described in Section III.G. The output I_{sp} will be used as an example. For this quantity the maximum residual was 0.84% of the I_{sp} at Mach 6 and dynamic pressure of 75kPa on the undeformed geometry. This reference I_{sp} is 2548.94 s. Using testing points, the maximum relative residual for the specific impulse was 1.94%. The associated R-squared value is 0.99956,

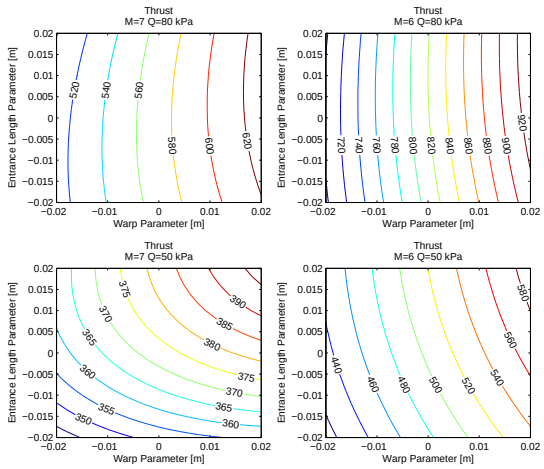

(a) Thrust estimate as calculated by a response surface at four freestream conditions.

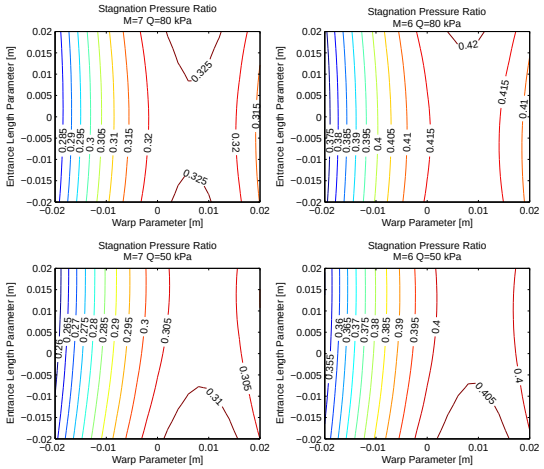

(b) Stagnation Pressure Ratio between freestream and end of the inlet/isolator (station 3) as calculated by a response surface at four freestream conditions.

Figure 15: Thrust and P_{tr} Contours

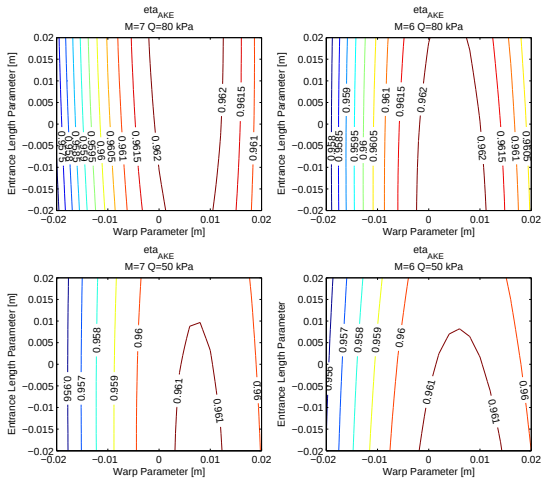

(a) Adiabatic Kinetic Energy Efficiency contours as calculated by a response surface at four freestream conditions.

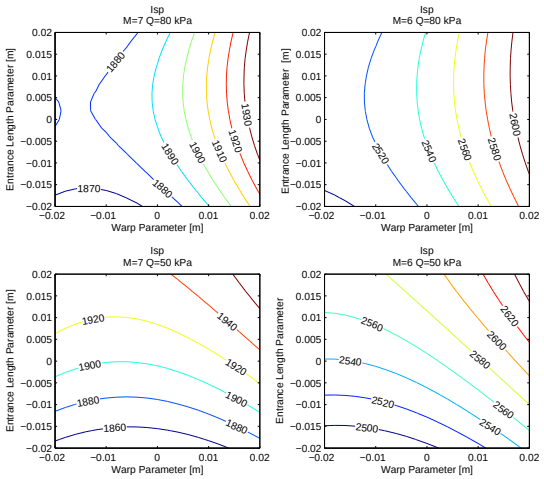

(b) Specific Impulse estimate as calculated by a response surface at four freestream conditions.

Figure 16: η_{AKE} and I_{sp} Contours

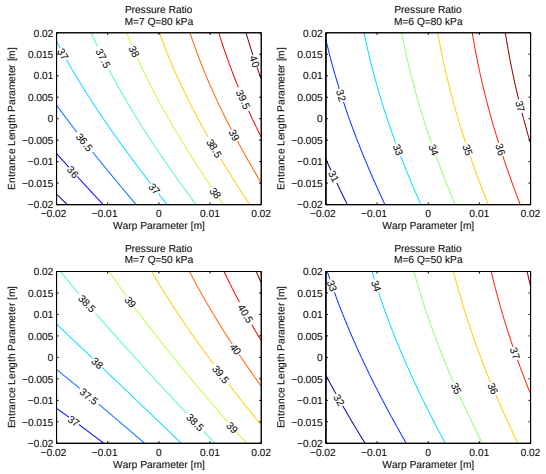

(a) Static Pressure Ratio between freestream and end of the inlet/isolator (station 3) as calculated by a response surface at four freestream conditions.

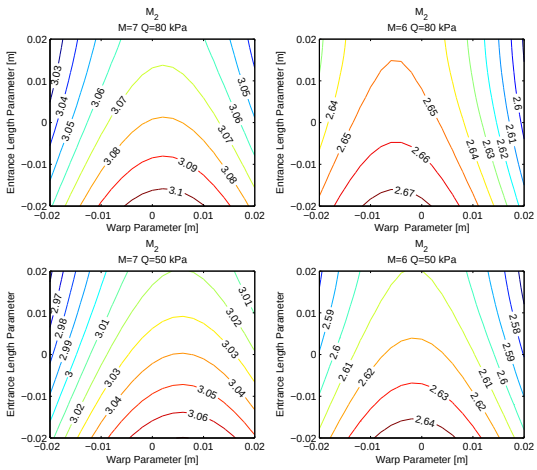

(b) Mach number at the end of the inlet/isolator (station 3) as calculated by a response surface at four freestream conditions.

Figure 17: Static Pressure Ratio and Mach number Contours

which indicates that the response surface is accounting for most of the variability in the specific impulse. A normal probability plot of the residuals is shown in Fig. 18. Most of the points lie along the normal probability line, however some divergence from that line indicates that the quadratic polynomial may not be the best model. The other quantities of interest discussed yield errors of a similar order of magnitude.

E. Performance Results

In this section we summarize the performance characteristics of the inlet under structural deformations and variations in freestream conditions. The temperature distribution was based on the temperature profile within the boundary layer near the wall at the centerline of the inlet, which is shown by the solid line if Fig 19. Assuming that the wall has been cooled to an average temperature of 300 ^{o}K and retains the same profile results in the dashed line in this figure. Based on the results of Ref. 21, the cooled wall temperature is likely to be of a similar shape to the uncooled wall. Differences between the temperature profile within the boundary layer and the temperature profile of the wall material due to uneven cooling or material thickness has been neglected. The initial temperature used in the structural model was 300^{o}K, meaning that the thermal expansion is determined by the difference between the temperature profile applied and this initial condition. This assumes that the manufacturer has built the vehicle such that it will hold the designed shape at the specified constant wall temperature. The average applied temperature was incremented by 5 degrees in additional cases, which had the same initial temperature.

Table 2 shows performance results using an Euler simulation. Euler simulations, conducted use SU^2, provide supplemental results which may indicate general trends. While the corresponding viscous simulations were attempted, significant difficulty was encountered due to the low quality of the deformed viscous meshes. For this reason, viscous results are limited to smaller-scale deformations. As the maximum deformation was observed to be nearly linear with respect to the average surface temperature, it is reasonable to assume that a stiffer structure or a smaller change in temperature can be approximated by a fraction of the computed deformation. A comparison of the viscous and inviscid results is summarized in Table 4. It can be seen here that the viscous model produces a predicted change in thrust in the same direction as the inviscid model, however of a significantly different magnitude. The baseline thrust prediction is also significantly different. This indicates that an inviscid model is not sufficient to predict the thrust of this type of scramjet. The results of the inviscid model suggest less than a Newton change in thrust per degree change in the temperature of the structure; however it appears that when viscous effects are included in the model of the inlet the sensitivity would be significantly higher.

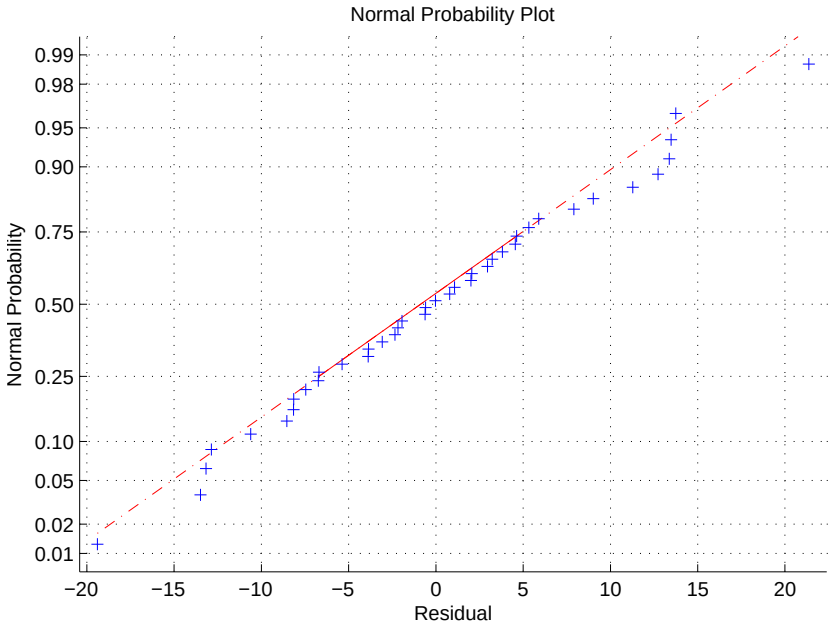

Figure 18: Normal probability plot of the residuals for specific impulse

Table 2: Inviscid Thrust Estimates. Structure deformed under initial pressure profile and temperature profile adjusted to have a desired average temperature.

Average Temperature [K]	Thrust [N]
no deformation	621.21832
290	589.69358
295	589.91661
300	587.07702
305	586.77566
310	586.47986

Table 3: Tip Deflection Results

Pressure	Temperature	Tip Deflection	
		x	z
Pressure, $q_\infty = 82kPa$	no change	2.14E-05	0.000165
Pressure, $q_\infty = 75kPa$	no change	1.939E-05	0.00015
Pressure, $q_\infty = 82kPa$	temperature profile - average of 300 degrees	-0.000984	-0.00778

Table 4: Comparison of Thrust Prediction with Viscous and Inviscid Models.

	Inviscid Model	Viscous Model	% change
Baseline geometry	621.21832 N	683.789 N	-9.151%
Pressure load only	622.11542 N	714.3914 N	-12.917%

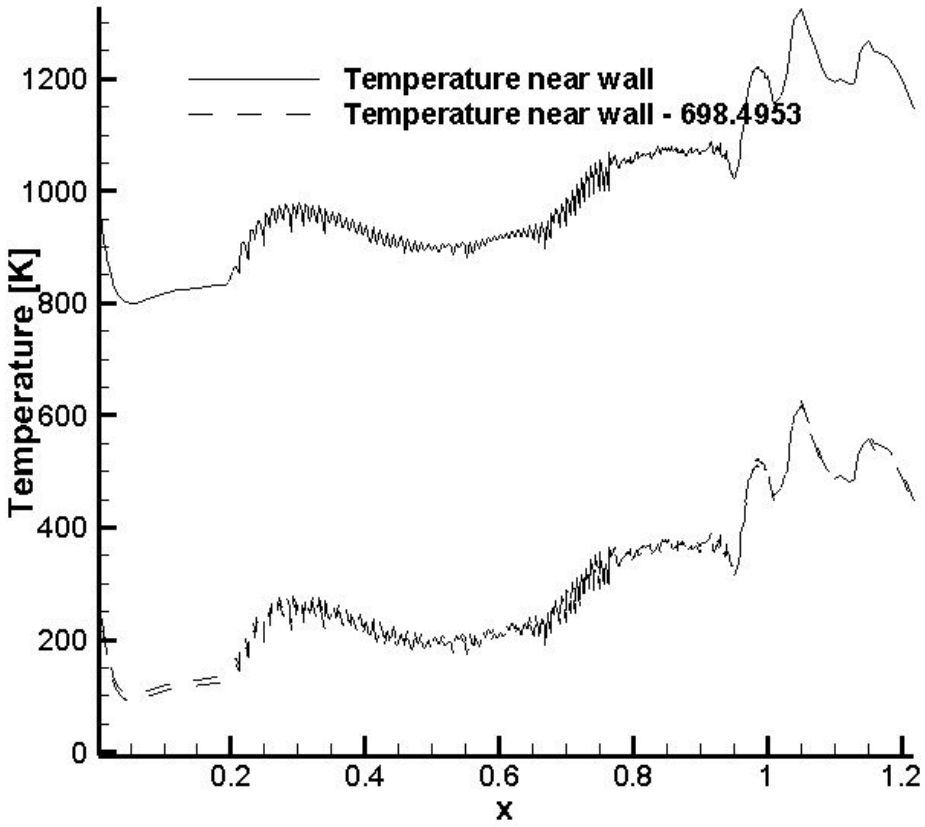

Figure 19: Temperature profile extracted from just below (1e-2m below) the upper surface of the inlet along the centerline. Dashed line indicates profile which has been adjusted to have an average temperature of 300 ^{o} K.

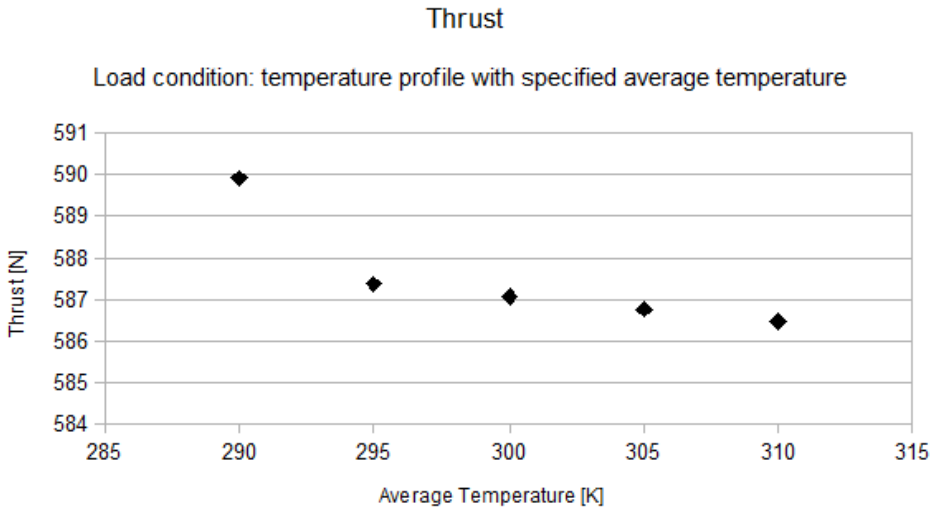

Figure 20: Inviscid thrust prediction plotted against average temperature of the applied temperature profile.

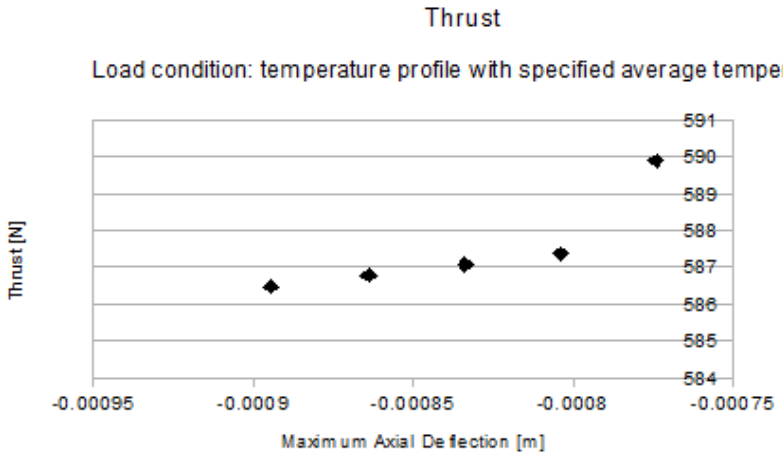

Figure 21: Inviscid thrust prediction plotted against maximum axial deflection of the structure.

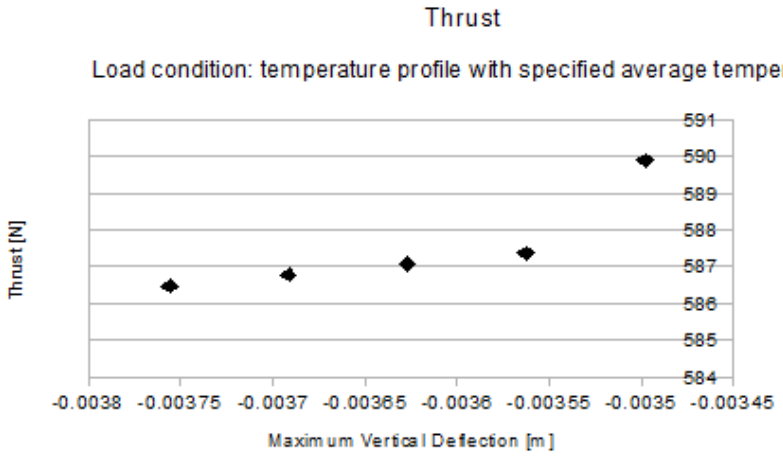

Figure 22: Inviscid thrust prediction plotted against maximum vertical deflection of the structure.

The trend observed in the thrust as predicted using inviscid, Euler simulations is a slight negative slope of 0.3 N per degree in the neighborhood of the central (300 degree) case. This is much smaller than the change observed between the baseline (undeformed) geometry and the deformed cases, which was on the order of 10% of the baseline thrust. As extreme temperature changes can be encountered in hypersonic flow (for example, there is a difference of 400 degrees between the two ends of the inlet) this may still be a significant effect, and the sensitivity may be much higher when viscous effects are taken into account. In addition, as shown in these plots, the sensitivity to average wall temperature may increase further away from the central average wall temperature.

The response surface for thrust can be used to compare to these results. A comparison of interest is the variation in performance due to manufacturing tolerances. The manufacturing tolerance on this type of inlet has been estimated as 0.00025 m.[22] This is of the same order as the difference between maximum deflection at the minimum and maximum average temperatures applied to the structural model. In order to obtain an estimate of the expected variation in thrust due to deformations of the size predicted by the structural model, a random distribution of deformations was input into the response surface equation. The random distribution for each of the three shape parameters was defined with a normal distribution with a mean of 0 and a variance of 2e-4. Using 1000 samples produced an output distribution of thrust which has a 99% confidence that the thrust will lie within +/- 10.2% of the mean thrust. This is on the same order as the change in thrust predicted by the viscous model. This indicates that the sensitivity of the thrust to structural deformations is of the same order of magnitude as the effect of manufacturing tolerances. As the viscous model predicts a larger change, once those effects are taken into account the effect of the structural deformations may dominate.

V. Conclusions

This paper focused on the effects of shape deformations on the performance of the vehicle inlet, and in particular on the deformations under pressure and temperature loads. A structural model was developed using the shape of the inlet and finding reasonable dimensions by optimizing for a minimum weight under constrained maximum stress. The load condition for the structure was based on CFD results, and the resultant deflections were applied to the CFD meshes and simulated to find an estimate of the change in thrust.

Comparable results were obtained between VULCAN and SU^2 despite differing mesh requirements. The 82kPa Mach 7 flight condition is temperature-dominated in terms of the structural deflections. Small aerothermoelastically determined deformations, with a magnitude of 1.65e-4 m vertical tip deflection produced a 4.5% change in thrust. Propagating a random distribution of prescribed deformations into a response surface developed from viscous simulations indicated 99% confidence interval bounds at +/- 10.2% of the mean thrust. Euler simulations, which are not reflective of the performance of this inlet due to the significance of viscous effects in hypersonic flow, indicate a lower sensitivity. Deflection of the nose in temperature-dominated cases was in the downward and upstream direction, and caused a decrease in thrust. Slight deflection of the nose upward in a pressure dominated case (where temperature change had been neglected) resulted in a slight increase in thrust.

These results show that deformations of the inlet should be taken into account in scramjet design, either through determining the deformation to a high degree of accuracy or designing so as to be robust to such uncertainties. Viscous effects are significant, and both the performance and the variation in performance will not be accurately predicted when simulating without viscous effects. It is a requirement for scramjets intended as launch vehicle propulsion that they must operate at a very wide range of conditions. This leads to a correspondingly wide range of pressure and temperature loads. As the temperature load dominated in this case, and as these vehicles are likely to increase in wall temperature during a flight, structural heating should be taken into account in multi-point optimization of scramjet inlet geometries.

There are several areas of further research which could be conducted. As this work has been conducted on a single geometry, it would be of interest to investigate whether the same trends hold for similar REST-class inlets, fully rectangular inlets, or other geometries. More detailed structural analysis, incorporating three-dimensional pressure and temperature loads, would produce more precise estimates of the change in performance. An additional factor which may be important is nonequilibrium effects within the boundary layer. The high temperatures observed within the boundary layer as simulated with the RANS equations indicate that some of the assumptions of said equations, like a constant ratio of specific heats and the

assumption of an ideal gas, may not be valid within the boundary layer. Nonuniformities in the flow entering the combustor, including thick boundary layers as well as swirling flow observed in some CFD solutions, effect fuel mixing and combustor efficiency - an effect which has not been taken into account in this work. Sensitivity calculations through the use of adjoints in SU^2 offer one avenue of reduced computational cost.

VI. Acknowledgements

This work was supported by a NASA Space Technology Research Fellowship. H. Kline would additionally like to acknowledge the support of the Hypersonic Airbreathing Propulsion Branch at NASA Langley in particular Shelly Ferlemann, the Aerospace Design Lab and Stanford University.

References

[1]Hank, J. M., Murphy, J. S., and Mutzman, R. C., "The X-51A Scramjet Engine Flight Demonstration Program," *15th AIAA International Space Planes and Hypersonic Systems and Technologies Conference*, , No. May, April 2008, pp. 1–13.

[2]Marshall, L., Bahm, C., Corpening, G., and Sherrill, R., "Overview With Results and Lessons Learned of the X-43A Mach 10 Flight," *AIAA/CIRA 13th International Space Planes and Hypersonics Systems and Technologies Conference*, May 2005, pp. 1–23.

[3]Jackson, K., Gruber, M., and Barhorst, T., "The HIFiRE flight 2 experiment: an overview and status update," *AIAA Paper*, , No. August, Aug. 2009.

[4]Gupta, K. K. and Voelker, L. S., "Aeroelastic Simulation of Hypersonic Flight Vehicles," *AIAA Journal*, Vol. 50, No. 3, March 2012, pp. 717–723.

[5]McNamara, J. J., Friedmann, P. P., Powell, K. G., Thuruthimattam, B. J., and Bartels, R. E., "Aeroelastic and Aerothermoelastic Behavior in Hypersonic Flow," *AIAA Journal*, Vol. 46, No. 10, Oct. 2008, pp. 2591–2610.

[6]Gupta, K., Choi, S., and Ibrahim, A., "Development of aerothermoelastic acoustics simulation capability of flight vehicles," *48th AIAA Aerospace Sciences Meeting*, , No. January, 2010, pp. 1–14.

[7]Anderson Jr., J. D., *Hypersonic and High-Temperature Gas Dynamics Second Edition*, AIAA Education Series, AIAA, Blacksburg, Virginia, 2nd ed., 2006.

[8]Smart, M. K., "How Much Compression Should a Scramjet Inlet Do?" *AIAA Journal*, Vol. 50, No. 3, March 2012, pp. 610–619.

[9]Ferlemann, P. G. and Gollan, R. J., "Parametric Geometry , Structured Grid Generation , and Initial Design Study for REST-Class Hypersonic Inlets," .

[10]Gollan, R. and Ferlemann, P., "Investigation of REST-class Hypersonic Inlet Designs," *17th AIAA International Space Planes and Hypersonic Systems and Technologies Conference*, April 2011.

[11]Baurle, R. A., "VULCAN Home Page," http://vulcan-cfd.larc.nasa.gov, Accessed: July 2013.

[12]Smart, M. K., "Design of Three-Dimensional Hypersonic Inlets with Rectangular-to-Elliptical Shape Transition," *Journal of Propulsion and Power*, Vol. 15, No. 3, May 1999, pp. 408–416.

[13]Palacios, F., Colonno, M., Aranake, A., Campos, A., Copeland, S., Economon, T., Lonkar, A., Lukaczyk, T., Taylor, T., and Alonso, J., "Stanford University Unstructured (SU2): An open-source integrated computational environment for multi-physics simulation and design," *51st AIAA Aerospace Sciences Meeting and Exhibit.*, Grapevine, TX, Jan. 2013.

[14]Special Metals Corporation, "INCONEL alloy 718SPF," 2004.

[15]Heiser, W. H. and Pratt, D. T., *Hypersonic Airbreathing Propulsion*, AIAA Education Series, AIAA, Washington, D.C., 1994.

[16]Smart, M. K., "Scramjets," *The Aeronautical Journal*, Vol. 111, No. 1124, 2007, pp. 605–619.

[17]Baurle, R. and Gaffney, R., "The Art of Extracting One-Dimensional Flow Properties from Multi-Dimensional Data Sets," *AIAA*, Jan. 2007, pp. 1–19.

[18]Cantwell, B. J., *Aircraft and Rocket Propulsion; Course Reader*, Stanford, CA, 2007.

[19]The MathWorks Inc., "Mathworks," http://www.mathworks.com/, Accessed: November 2013.

[20]Optimal Solutions Software LLC, "Optimal Solutions," http://gosculptor.com/, Accessed: November 2013.

[21]Saito, T., Ono, F., Hayasaka, O., and Ueda, S., "Heating evaluation test of a duct-shaped cooling structure simulating scramjet combustors," *AIAA Paper*, , No. July, 2004, pp. 1–6.

[22]Ferlemann, S.

VII. Response Surface Coefficients

In the following table x_1, x_2 and x_3 refer to the shape parameters of the change in entrance length, central ridge, and warp respectively. The variables x_4 and x_5 refer to the Mach number and dynamic

pressure respectively. Each parameter has been normalized by its lower bound and range.

$$
\begin{aligned}
x_1 &= \frac{dEL + 0.02}{0.04} \\
x_2 &= \frac{C + 0.02}{0.04} \\
x_3 &= \frac{W + 0.02}{0.04} \\
x_4 &= \frac{M - 5}{2} \\
x_5 &= \frac{q - 50 * 10^3}{50 * 10^3}
\end{aligned}
\tag{6}
$$

Table 5: Response Surface Coefficients

	Thrust	I_{sp}	$P_{tr,cp}$	A_0	η_{AKE}
1	578.7556	3266	0.4418	0.009	0.9505
x_1	58.9462	120.2	-0.0029	0.0006	0.0001
x_2	-11.9098	-79.9	0.1404	0.0006	0.0148
x_3	228.6249	21.3	0.1778	0.0037	0.0176
x_4	-404.914	-1648.3	-0.1451	0.0029	0.0036
x_5	665.9072	46.6	0.0457	0.0004	0.0042
x_1x_2	19.2194	34.7	-0.0186	-0.0002	-0.002
x_1x_3	21.7852	17.3	0.004	0.0001	-0.0004
x_1x_4	-26.613	-8.9	-0.0029	-0.0002	0.0011
x_1x_5	-53.6006	-132.8	0.0098	-0.0002	0.0008
x_2x_3	25.6599	23.7	-0.0278	0.0003	-0.0036
x_2x_4	-1.5183	8.3	0.0007	0.0001	-0.0012
x_2x_5	43.7427	26.1	-0.0215	0.0001	-0.0031
x_3x_4	-217.054	-88.9	-0.0045	-0.0002	0.0019
x_3x_5	154.9537	52.3	-0.0149	0.0001	-0.0019
x_4x_5	-381.396	1.3	0.0077	-0.0004	0.0006
x_1^2	-22.6165	-45.1	0.0083	-0.0002	-0.0002
x_2^2	-4.3906	61.2	-0.0963	-0.0004	-0.01
x_3^2	-10.8625	72.9	-0.1107	-0.001	-0.0128
x_4^2	176.3218	257.6	-0.0072	-0.0001	-0.0033
x_5^2	-39.0462	-67.8	-0.0116	-0.0001	-0.0006